

Supplementary Information for

Dissecting pigment architecture of individual photosynthetic antenna complexes in solution

Quan Wang and W. E. Moerner*

Department of Chemistry, Stanford University, Stanford, CA 94305

*Correspondence to: W. E. Moerner, e-mail: wmoerner@stanford.edu

SI Materials and Methods

Preparation of APC in different aggregation states Monomers of APC were prepared from wild-type trimers (Prozyme, PB20, from *Spirulina sp.*). The sample was checked by SDS-PAGE to rule out contamination of other proteins (Fig. S3A). Spontaneous dissociation of the trimers into monomers were induced by diluting the sample to ~1nM concentration in PBS buffer and let sit for at least 15 hours. A pure monomer population was confirmed by bulk emission spectra (Fig. S3B), measurement of single-molecule transport coefficients (1) and mapping the brightness and emission spectrum of the initial level (Fig. S3D). For the study of trimers, crosslinked APC (Prozyme, PB25, also from *Spirulina sp.*) complexes were used to prevent dissociation at ~pM concentration. Denaturing SDS-PAGE showed that most subunits were crosslinked (Fig. S3A) and the percentage of trimers measured in the single-molecule experiments were estimated to be more than 90% by transport coefficients (1) as well as brightness-spectrum mapping of the initial level (Fig. S3 E and F). Molecules that showed “monomer-like” initial brightness and spectrum were not selected for further analysis in the trimer experiment. In order to assess the effect of crosslinking, we found that wild-type trimers can be measured at the single-molecule level following immediate dilution of non-crosslinked sample (Fig. S3C) and show highly similar photophysical properties compared to the crosslinked variant (Fig. S3B Table). This suggests that perturbation induced by crosslinking is minimum and is consistent with a previous bulk-level study (2). Trapping experiments were performed at ~10pM protein concentrations in 1× PBS buffer with 20% glycerol and ambient oxygen.

The Anti-Brownian ELectrokinetic (ABEL) trap The ABEL trapping apparatus (Fig. S1) was similar to that previously described (3). Specifically, a CW 594 nm He-Ne laser (Meredith Instruments) was used as the excitation source. The focused laser spot underwent a “knight’s tour” scanning pattern (Fig. S1 inset) on the sample plane that encodes position of the single molecule on the timing of each detected fluorescence photon. The photon-tagged position estimates were processed by a Kalman filter implemented on an FPGA (National Instruments, PCIe-7842R) to obtain near-optimal tracking of Brownian motion (4, 5). Appropriate voltages were subsequently applied to the microfluidic cell to actuate feedback forces in the x-y plane. An all-quartz microfluidic trapping cell with a z-channel depth of ~600 nm was used.

Multiparameter fluorescence detection Fluorescence emission spectra were measured on a Si EMCCD camera (Andor iXon 860) by dispersing ~50% of the signal photons via an Amici prism (Edmund Optics, NT42-586) after the confocal pinhole. Spectral frames were recorded at 50-ms time resolution. Before use, the spectrometer was first calibrated using discharge from a He-Ne tube. To measure single-molecule fluorescence polarization, a linear polarizer was inserted into

the excitation path to produce polarized excitation with an extinction >100:1. Collected fluorescence was separated into parallel and perpendicular channels by a polarizing beam splitter. For antibunching experiments (Fig. S7), the detection path consisted of a 50:50 non-polarizing beam splitter and a pair of avalanche photodiodes (PicoQuant, τ -SPAD) (6). To suppress crosstalk between the two channels as a result of broadband “avalanche re-emission” of the detectors (7), it was necessary to place bandpass filters right before each detector. To measure excited-state lifetime, we used an optical parametric oscillator (Coherent Mira-OPO) tuned to 594 nm as the excitation source to trap while simultaneously conducting time-correlated-single-photon-counting on single proteins (8). Time-resolved data for both antibunching and excited-state lifetime were recorded on a PicoHarp 300 (PicoQuant) timing module with 4ps resolution. More details of the instrumentation can be found in ref. (9).

Data analysis Photodynamics of individual molecules were analyzed on the basis of brightness levels identified by a change-point finding algorithm (10). Brightness was defined as the average number of detected photons per time bin (5 ms in this work). Spectral frames within a level were pooled and background subtracted to yield the average spectrum associated with the brightness level. Spectra were characterized by the “center-of-mass” (CM),

$$\bar{\lambda}_m = \frac{\sum_k I_k \lambda_k}{\sum_k I_k} \quad (\text{S1})$$

where I_k is the signal of the wavelength bin centered at λ_k . The spectral CM provides a more robust metric for detecting small spectral shifts at low signal-to-background conditions compared to fitting. The shot-noise limited variance associated with $\bar{\lambda}_m$ can be calculated by applying the error propagation rule to Eq. (S1) to yield

$$\text{var}(\bar{\lambda}_m) = \sum_k \left(\frac{\lambda_k \sum I_k - \sum I_k \lambda_k}{(\sum I_k)^2} \right)^2 \text{var}(I_k) \quad (\text{S2})$$

where the variance of each spectral bin ($\text{var}(I_k)$) was estimated by converting the signal to the number of photons and accounting for the factor of 2 excess noise produced in the electron-multiplication process ($\text{var}(I_k) = 2(I_k + b_k)$, b_k is the background count in spectral bin k). At times, for maximum time resolution, the spectral CM of each frame was plotted (Fig. 2 and Fig. S8). The error bars associated with the spectral CM of a brightness level were calculated as follows: if the level contained multiple frames ($n > 1$), the standard error of the mean (σ_{CM} / \sqrt{n}) was used, if the level contained only one frame, the shot-noise limited uncertainty (Eq.(S2)) was used. Excited-state lifetime was extracted by fitting the delay-time histogram to the following equation:

$$g(t; \tau, c) = (1 - \gamma) \left[\text{IRF}(t - c) \otimes \exp\left(-\frac{t}{\tau}\right) \right] + \gamma g_{BG}(t) \quad (\text{S3})$$

where γ is the background fraction, $g_{BG}(t)$ is the experimentally measured decay histogram from background photons, $\text{IRF}(t)$ is the instrument response function, \otimes indicates convolution, c is the time shift of the IRF and τ is the excited-state lifetime. The maximum likelihood method (11) was used to correctly account for the Poisson statistics of photon counting. Fluorescence antibunching curves (brightness correlation on a ~ns timescale, Fig. S7) were constructed by cross correlating (12) the two channels in a linear time lag region of -30 – +30 ns. Antibunching curves were fitted with the following function to extract the (apparent) number of independent emitters (n)

$$g(t, n, c) = \left[1 - \frac{1}{n} \exp\left(-\frac{|t|}{\tau}\right) \right] \otimes \text{IRF} \quad (\text{S4})$$

where τ is the rise time constant and the IRF is the instrument response function (~ 0.3 ns) measured by constructing a start-stop histogram of a pulsed laser. More details of the analysis can be found in ref. (9).

Single-molecule fluorescence polarization

Analysis The emission polarization was calculated as

$$\text{FPol} = \frac{(S_{\parallel} - b_{\parallel}) - (S_{\perp} - b_{\perp}) / g}{(S_{\parallel} - b_{\parallel}) + (S_{\perp} - b_{\perp}) / g} \quad (\text{S5})$$

where S and b are the signal and background of the corresponding polarization detection channels and g is a pre-calibrated factor that accounts for the difference in detection efficiency between the two channels. The shot-noise limited uncertainty can be estimated by applying the standard error propagation rules to Eq. (S5), similar to previous work (13)

$$\text{var}(p) = \frac{4(S_{\perp} - b_{\perp})^2 S_{\parallel}}{I_{\text{tot}}^4 g^2} + \frac{4(S_{\parallel} - b_{\parallel})^2 S_{\perp}}{I_{\text{tot}}^4 g^2} \quad (\text{S6})$$

where $I_{\text{tot}} \equiv (S_{\parallel} - b_{\parallel}) + (S_{\perp} - b_{\perp}) / g$ is the total (corrected) signal. The system g factor was calibrated to be 0.87, by comparing the measured FPol values at two orthogonal excitation polarizations on the same fluorescent sample (9). FPol of a single-molecule trace was calculated either from every 150 total detected photons, or from all photons associated with a brightness level. The error bars were quoted as s.e.m., if the brightness level contained multiple FPol estimates (150 photons in each estimate) or calculated using Eq. (S6), if a brightness level contained fewer than 150 photons.

Effects of high NA optics It is well known that the high numerical aperture (NA) optics used in a fluorescence microscope lowers the contrast of measured fluorescence polarization (14, 15). In our study it is critical to quantitatively estimate this effect.

We start by using the parallel and perpendicular components of an emission dipole derived by Fourkas (16).

$$\begin{aligned} I_{\parallel}^{\Theta, \Phi} &= I_{\text{tot}} \left(A + B \sin^2 \Theta + C \sin^2 \Theta \cos 2\Phi \right) \\ I_{\perp}^{\Theta, \Phi} &= I_{\text{tot}} \left(A + B \sin^2 \Theta - C \sin^2 \Theta \cos 2\Phi \right) \end{aligned} \quad (\text{S7})$$

where Θ and Φ specify the orientation of an emission dipole (Fig. S2A), A , B and C are functions of the collection NA (17) (or equivalently parameterized by the half angle α)

$$\begin{aligned} A &= \frac{1}{6} - \frac{1}{4} \cos \alpha + \frac{1}{12} \cos^3 \alpha \\ B &= \frac{1}{8} \cos \alpha - \frac{1}{8} \cos^3 \alpha \\ C &= \frac{7}{48} - \frac{1}{16} \cos \alpha - \frac{1}{16} \cos^2 \alpha - \frac{1}{48} \cos^3 \alpha \end{aligned} \quad (\text{S8})$$

Next, we calculate the integrated response of Eq. (S7) due to rotational averaging in the presence of photo-selection. Assuming that the excitation polarization is along the x axis (Fig. S1), we apply

a weighting factor proportional to $|\vec{\mu} \cdot \vec{E}|^2 \propto \cos^2 \Phi \sin^2 \Theta$ and integrate Eq. (S7) over the full solid angle

$$\begin{aligned} I_{\parallel} &= \int_0^{2\pi} \int_0^{\pi} I_{\parallel}^{\Theta, \Phi} \cos^2 \Phi \sin^2 \Theta \sin \Theta d\Theta d\Phi \\ I_{\perp} &= \int_0^{2\pi} \int_0^{\pi} I_{\perp}^{\Theta, \Phi} \cos^2 \Phi \sin^2 \Theta \sin \Theta d\Theta d\Phi \end{aligned} \quad (\text{S9})$$

The resulting FPol as a function of the NA of the detection optics can be calculated numerically using

$$\text{FPol}(\alpha) = \frac{I_{\parallel}(\alpha) - I_{\perp}(\alpha)}{I_{\parallel}(\alpha) + I_{\perp}(\alpha)} \quad (\text{S10})$$

and this function is plotted in Fig. S2B. Using a water immersion objective lens with NA = 1.2 reduces the maximum FPol from 0.5 to ~0.42.

Interpretation of FPol Common sources of depolarization in an FPol experiment include internal relaxation, rotational diffusion and energy transfer (18). In our experiments, given the observation that the single-pigment states all displayed FPol values very close to the theoretical value of a single dipole emitter (when high NA effects are properly accounted for), we conclude that internal relaxation does not contribute significantly to the measured FPol.

On the other hand, the amount of depolarization due to rotational diffusion can be estimated using Perrin's equation as follows,

$$\frac{r(t_{rot})}{r_{max}} = \frac{1}{1 + \tau / t_{rot}} \quad (\text{S11})$$

where r_{max} is the maximum anisotropy without rotational diffusion, τ is the fluorescence lifetime and t_{rot} is the rotational correlation time. For APC in PBS buffer containing 20% glycerol, the rotation correlation time is estimated to be about ~20 ns (18), which is much longer than the excited-state lifetime (~1 ns). Consequently, rotational diffusion only causes a minor (5% for β , 7% for α) reduction of FPol. For APC trimers, the effect is even smaller (~3%) due to the longer rotational diffusion time (~60 ns).

We thus interpret FPol in our experiments as reflecting the routes of energy transfer between pigments. Considering both high NA and rotational diffusion effects, the maximum value of FPol is estimated to be ~0.40 for monomers and ~0.41 for trimers.

FRET calculations

Rates of energy transfer were calculated using the classical FRET equation (19)

$$k_{DA} = \frac{\Phi_D k_D^{10} \kappa^2}{R_{DA}^6} \left(\frac{9000 \ln 10}{128 \pi^5 N_A n^4} \right) \frac{\int F_D(\lambda) \epsilon_A(\lambda) \lambda^2 d\lambda}{\int F_D(\lambda) \lambda^{-2} d\lambda} \quad (\text{S12})$$

The refractive index was assumed to be 1.4 in all calculations.

Energy transfer within a FRET network

Energy transfer within a FRET network that contains N sites was modeled by the following master equation

$$\frac{d\mathbf{p}(t)}{dt} = \mathbf{M}\mathbf{p}(t) \quad (\text{S13})$$

where $\mathbf{p}(t)$ is a $N \times 1$ vector that represents the probability of finding a quanta of excitation energy in each of the system's N sites following an absorption event. \mathbf{M} is the transition matrix with off-diagonal elements representing energy transfer rates

$$M_{ij} = K_{j \rightarrow i} \quad (i \neq j) \quad (\text{S14})$$

and diagonal elements representing total decay rates of the individual sites

$$M_{ii} = -\left(k_i^{10} + \sum_{j, i \neq j} K_{i \rightarrow j} \right) \quad (\text{S15})$$

where k_i^{10} is the excited-state decay rate of site i . Eq. (S13) was solved by consecutively initializing the system at the individual sites (i.e. $\mathbf{p}^j(0) = [\dots, 0, p_j = 1, 0, \dots]^T$). Here, we assume the maximum number of excitation quanta in the system to be one at any given time. This is reasonable because the probability of a second absorption event during the excited-state lifetime of the first quanta is low in our experiment (<3%). Each solution set $\mathbf{p}^j(t)$ represents the time-dependent probability of being in the excited state for all the individual sites, after a quanta of excitation energy enters the system from site j . Measurable fluorescence parameters, including brightness, FPol, apparent excited-state lifetime and emission spectrum, can be subsequently calculated using $\mathbf{p}^j(t)$ and the site properties.

Specifically, the total brightness is simply the sum of the site brightness values

$$B = \sum_i B_i \quad (\text{S16})$$

which can be calculated by

$$B_i = \sum_j A_j P_i^j \quad (\text{S17})$$

P_i^j is the probability of fluorescence emission from site i when the initial absorption happens through site j .

$$P_i^j \equiv \int_0^{+\infty} p_i^j(t) k_i^{10} \Phi_i dt \quad (\text{S18})$$

Here, A_i and Φ_i are the absorption probability and quantum yield, respectively, of site i .

Fluorescence anisotropy can be calculated by considering all possible combinations in which a quanta of excitation energy enters the system and leaves via fluorescence emission (20).

$$r = \sum_j A_j \left(\frac{\sum_i r_{ji} P_i^j}{\sum_i P_i^j} \right) / \sum_j A_j \quad (\text{S19})$$

r_{ij} is the fundamental anisotropy that links site i and j and was calculated from the angular separation (θ_{ij}) of the two dipoles.

$$r_{ij} = r_{ji} = \frac{2}{5} \left(\frac{3 \cos^2 \theta_{ij} - 1}{2} \right) \quad (\text{S20})$$

Finally, anisotropy is converted to FPol by

$$\text{FPol} = \frac{3r}{r+2} \quad (\text{S21})$$

Time-resolved fluorescence decay can be constructed by averaging all emissive sites in the system, weighted by their relative brightness values.

$$g(t) = \sum_i \Phi_i k_i^{10} \left(\frac{\sum_j A_j p_i^j(t)}{\sum_j A_j} \right) \quad (\text{S22})$$

The emission spectrum can be calculated by averaging the spectra of the individual sites, weighted by their brightness values.

$$S(\lambda) = \frac{\sum_i B_i S_i(\lambda)}{\sum_i B_i} \quad (\text{S23})$$

SI Results and Discussion

Fluorescence antibunching measurement to probe singlet-singlet annihilation

FRET-type energy transfer between two *excited states* has been found to be a common feature in a number of natural (21, 22) and artificial antennas (23). This is also known as singlet-singlet annihilation (SSA) because effectively one potential fluorescence photon is quenched (e.g. $S_1^a + S_1^b \rightarrow S_0^a + S_n^b \rightarrow S_0^a + S_1^b$). To investigate if SSA is present in APC monomers, we conducted photon antibunching measurements (Fig. S7), similar to measurements on immobilized (24) or tracked molecules (25), on trapped monomer proteins in solution. Essentially, the depth of the photon antibunching dip would decrease in the presence of SSA. Given that the trapped single complexes proceeded through different brightness levels as shown in Fig. S7A, we were able to group the inter-photon delay times appropriately to extract separate correlation curves for the various states. We found that the intact $\alpha+\beta$ state (monomer) gave an antibunching signal consistent with efficient SSA between the α and β pigments. This is in line with the favorable spectral overlap between the S_1 absorption and S_1 emission on the monomer, as revealed by pump-probe studies (26, 27). Similar SSA processes between constituent chromophores were also found in the tetrameric fluorescent protein DsRed (28).

Implications for OCP-mediated photoprotection mechanism in cyanobacteria

Recently, APC was found to be an important player in the non-photochemical quenching pathway of cyanobacteria, mediated by the orange carotenoid protein (OCP). OCP, upon absorption of blue light, can photo-convert into a red form (OCPr) which binds to APC in the core of the antenna supercomplex (the phycobilisome) (29). It has been established that OCPr acts by creating a quenching site of the 660 nm emission in the phycobilisome (30), but the specific site and mechanism of quenching remains undetermined. Based on our spectroscopic model, the site of 660 nm emission corresponds to the α pigment, which is located at the exterior of the protein. It is possible that OCPr binds in close proximity to the α pigment to directly quench its excited state, as proposed by two recent structural studies (31, 32). On the other hand, our data indicates that the β pigment from a neighboring monomer is a photoactivatable quenching site that efficiently dissipates excitation energy of the whole complex. Given the higher degree of conformational flexibility of the β pigment in its binding pocket, as revealed by our monomer data, it is also possible that OCPr activates quenching through an induced conformation rearrangement of the β pigment upon binding (33).

SI Figures

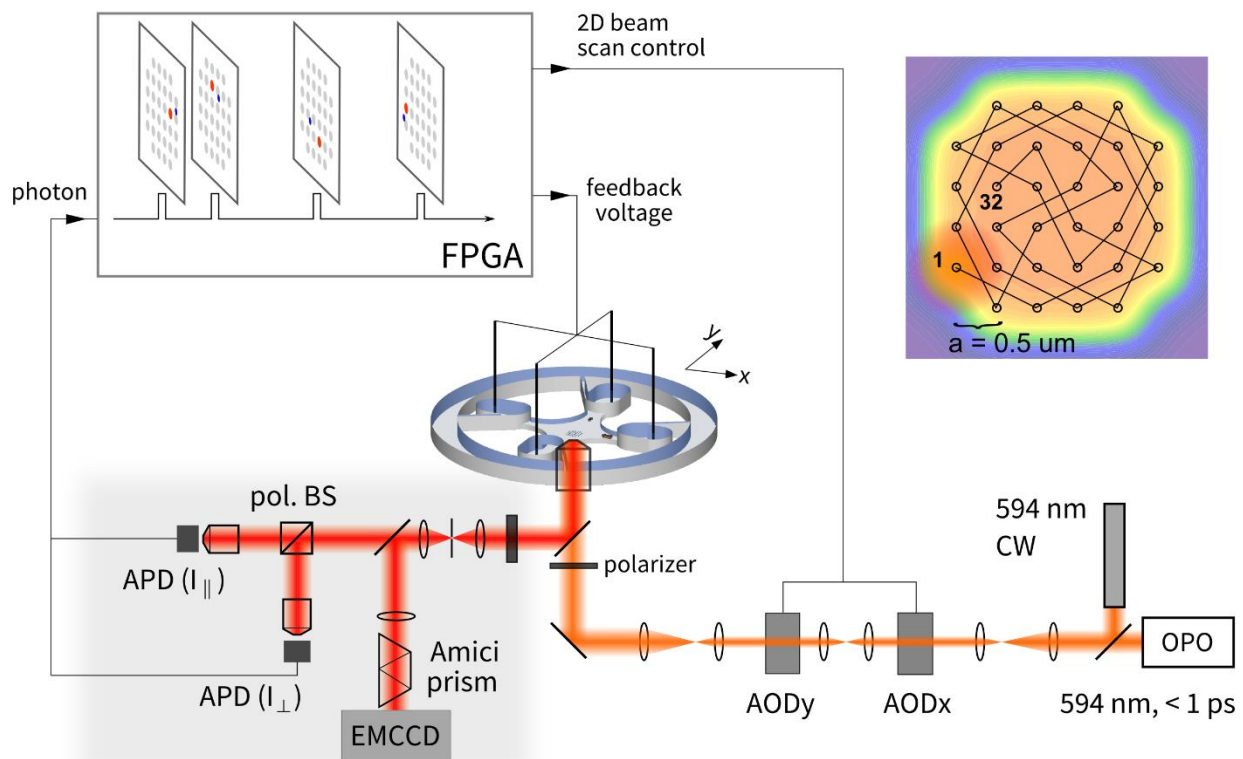


Fig. S1. Detailed experimental setup including the position-sensitive excitation scheme (inset), feedback block diagram, the microfluidic chamber and polarization-sensitive, multiparameter fluorescence detection.

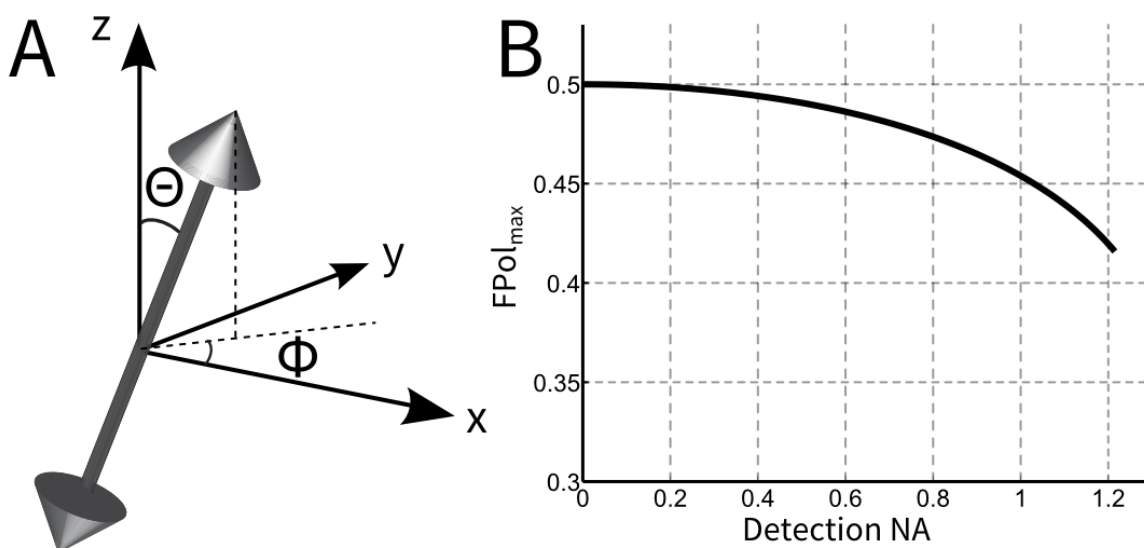


Fig. S2. Effects of detection numerical aperture (NA) on fluorescence polarization contrast. (A) Coordinate system of a single dipole emitter in sample space. (B) Calculated maximum FPol contrast (using Eqs. (S7)-(S10)) as a function of detection NA.

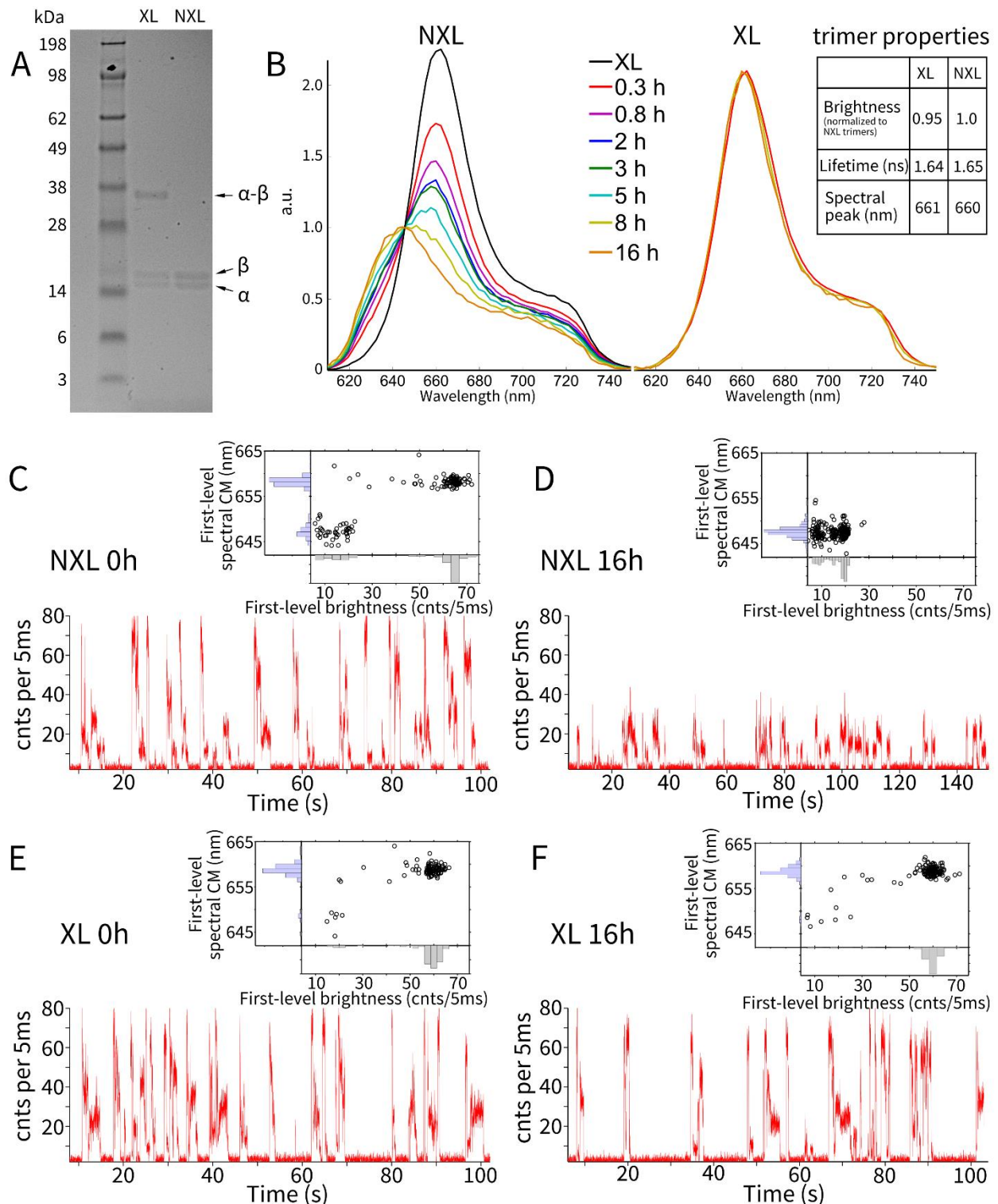


Fig. S3. Biochemical and biophysical characterizations of APC samples used in this work. (A) SDS-PAGE gel of crosslinked APC (XL) and wild-type APC (NXL). (B) Time-dependent APC dissociation probed by ensemble emission spectra. Proteins were diluted to ~ 1 nM concentration in 30mM HEPES buffer and the emission spectra were measured at specified time points using the Amici-prism based spectrometer. Inset: photophysical properties of XL and NXL trimers. Data were acquired from single-molecule experiments by pooling photons from the pristine trimer state. (C-F) Example single-molecule brightness traces at different experimental conditions. Insets show

mapping of first-level brightness and emission spectrum of each molecule. All experiments were done at the same excitation power. (C) Wild-type APC measured immediately after dilution from a $\sim 4\mu\text{M}$ stock. (D) Wild-type APC after 16h of spontaneous dissociation at $\sim 1\text{nM}$ in 30mM HEPES. (E) XL APC measured immediately after dilution from a $\sim 4\mu\text{M}$ stock. (F) XL APC after 16h of spontaneous dissociation at $\sim 1\text{nM}$ in 30mM HEPES.

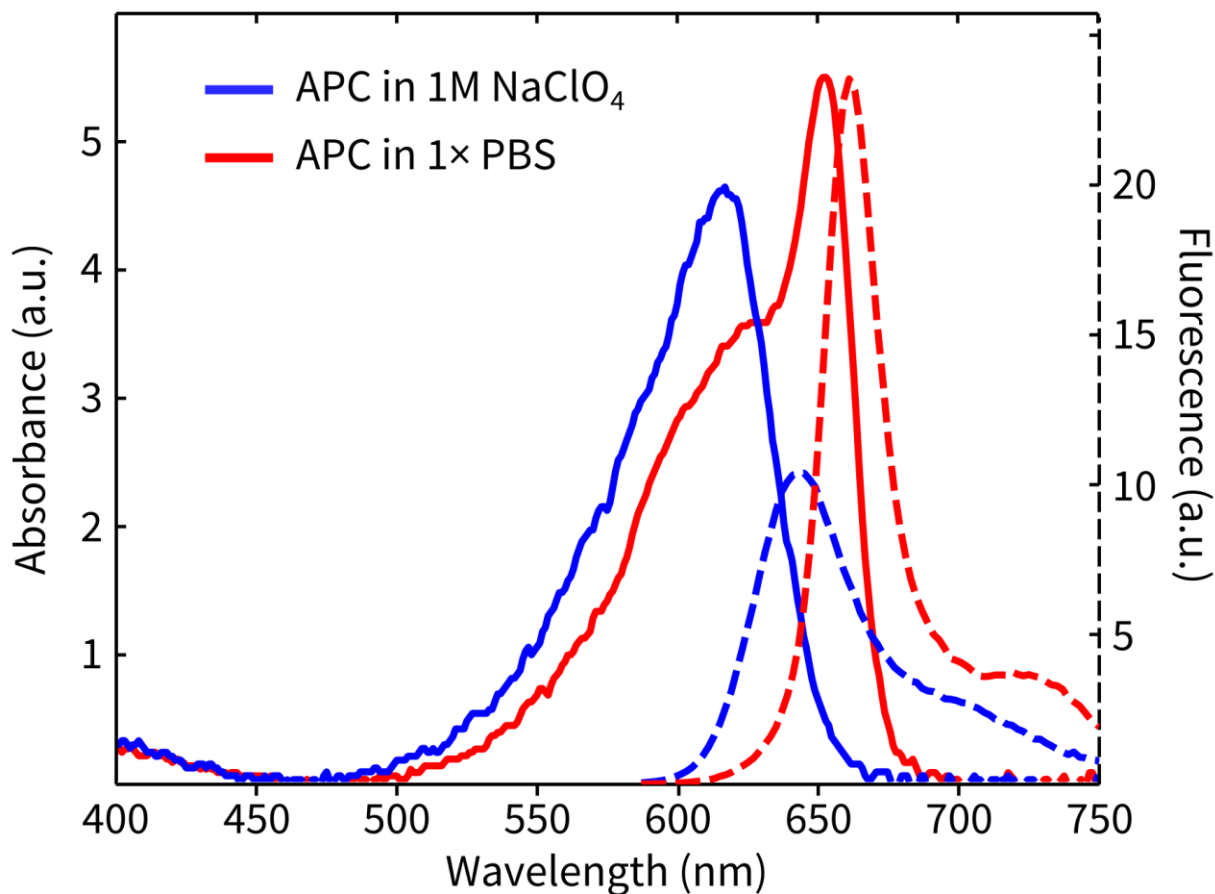


Fig. S4. Ensemble spectra of Allophycocyanin (*Spirulina sp.*). APC in 1M NaClO_4 presumably represents dissociated monomers. The two absorption curves are normalized at A_{280} .

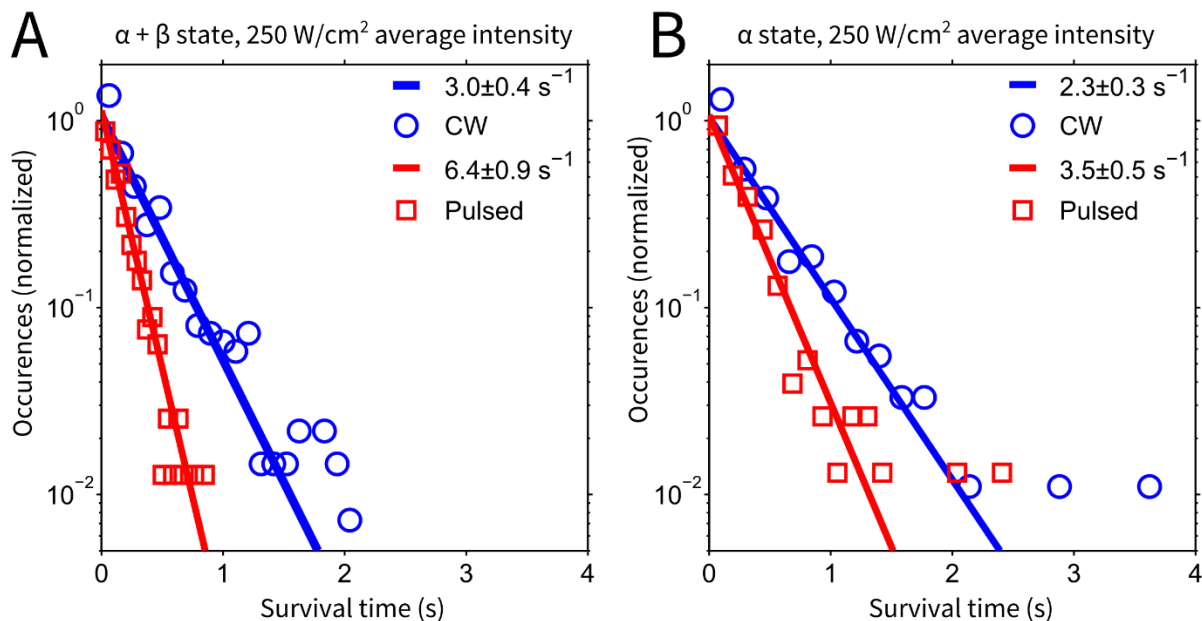


Fig. S5. Photodegradation rates under CW and pulsed excitation conditions. (A) Survival time histograms of the intact monomer ($\alpha+\beta$ state) with single exponential fits to extract photodegradation rates. (B) Survival time histograms of the α -only state with single exponential fits to extract photodegradation rates.

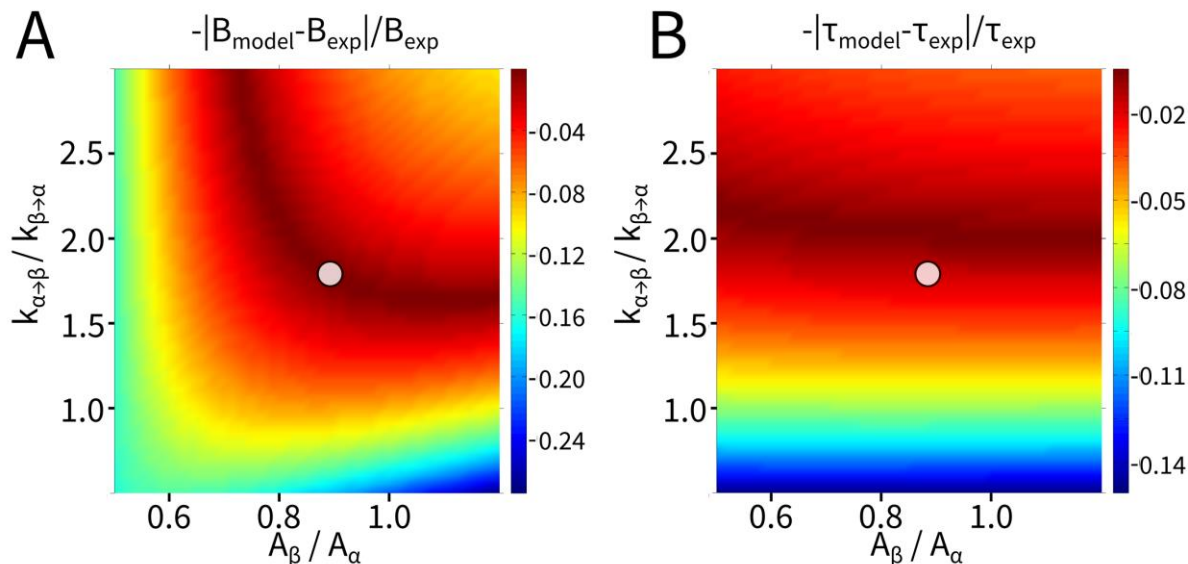


Fig. S6. Extracting ratios of energy transfer rates ($k_{\alpha\rightarrow\beta}/k_{\beta\rightarrow\alpha}$) and absorption probability (A_{β}/A_{α}) of the monomer from minimizing the differences between modeled and measured parameters of the intact monomer. (A) Difference map of fluorescence brightness. (B) Difference map of excited-state lifetime. Red regions represent good agreement between model and experiment. Values marked with a white circle are consistent with a FRET equation calculation (see main text) and are used in quantitative modeling.

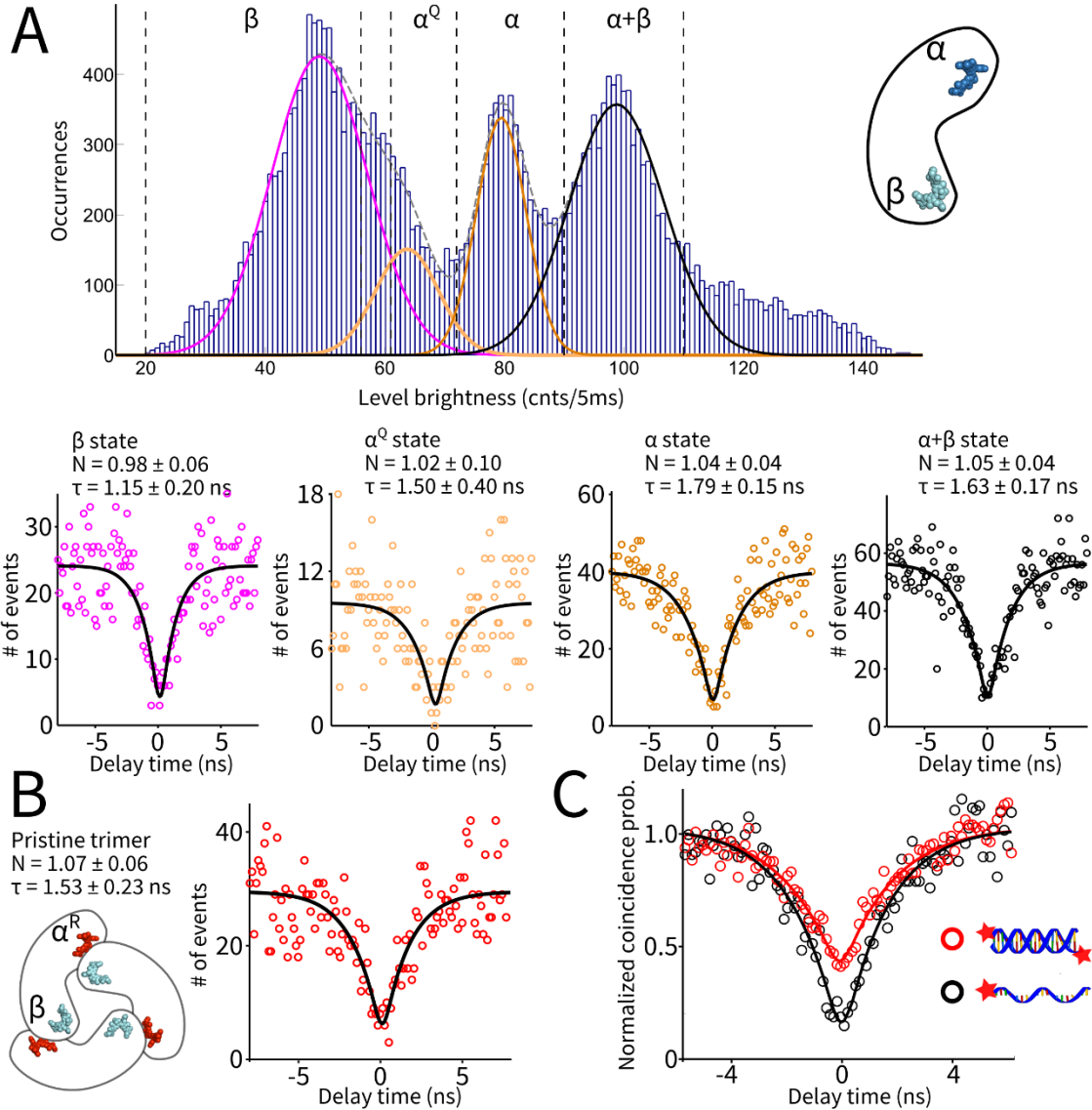


Fig. S7. Fluorescence antibunching measurements on APC. (A) Antibunching signal from the four emissive states of monomer, which were identified in this experiment by fitting the fluorescence brightness histogram with a sum of four Gaussians. Brightness levels that exceeded 110 cnts/5ms were due to transient (<50ms) co-occupation of two molecules in the trap and the photons from these short-lived levels (<1%) were not analyzed. Photons from each brightness state, as defined by the dashed lines, were used to construct the corresponding antibunching histograms. The apparent number of independent emitters (N) and rise time constant (τ) of each state were extracted by fitting the antibunching correlation with Eq. (S4). (B) Antibunching signal from the pristine trimer state with 6 intact pigments. (C) Control experiments with DNA molecules. Red: antibunching signal from trapped double-stranded DNA molecules (30nt) that contains two Cy5 dyes at opposite ends. Black: antibunching signal from trapped single-stranded DNA molecules (30nt) that contains only one Cy5 dye at the 5' end. The small but non-zero coincidence probability at zero delay is mainly due to the limited time resolution of the detectors (~ 0.3 ns).

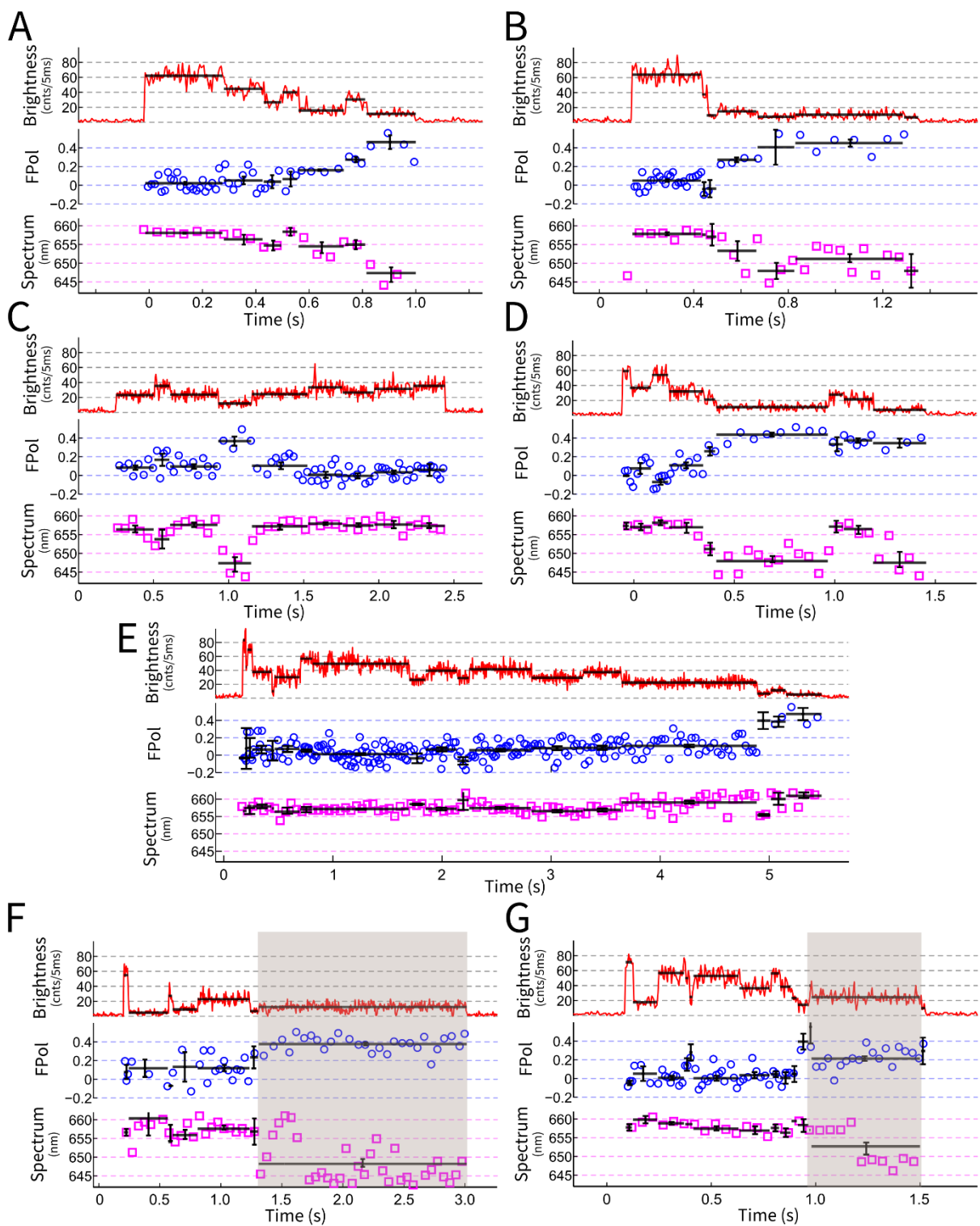


Fig. S8. More examples of trimer photodynamics probed in the ABEL trap with multi-parameter fluorescence spectroscopy. Shaded regions in *F* and *G* highlight levels that show large spectral blue shifts without significant changes in brightness and FPol.

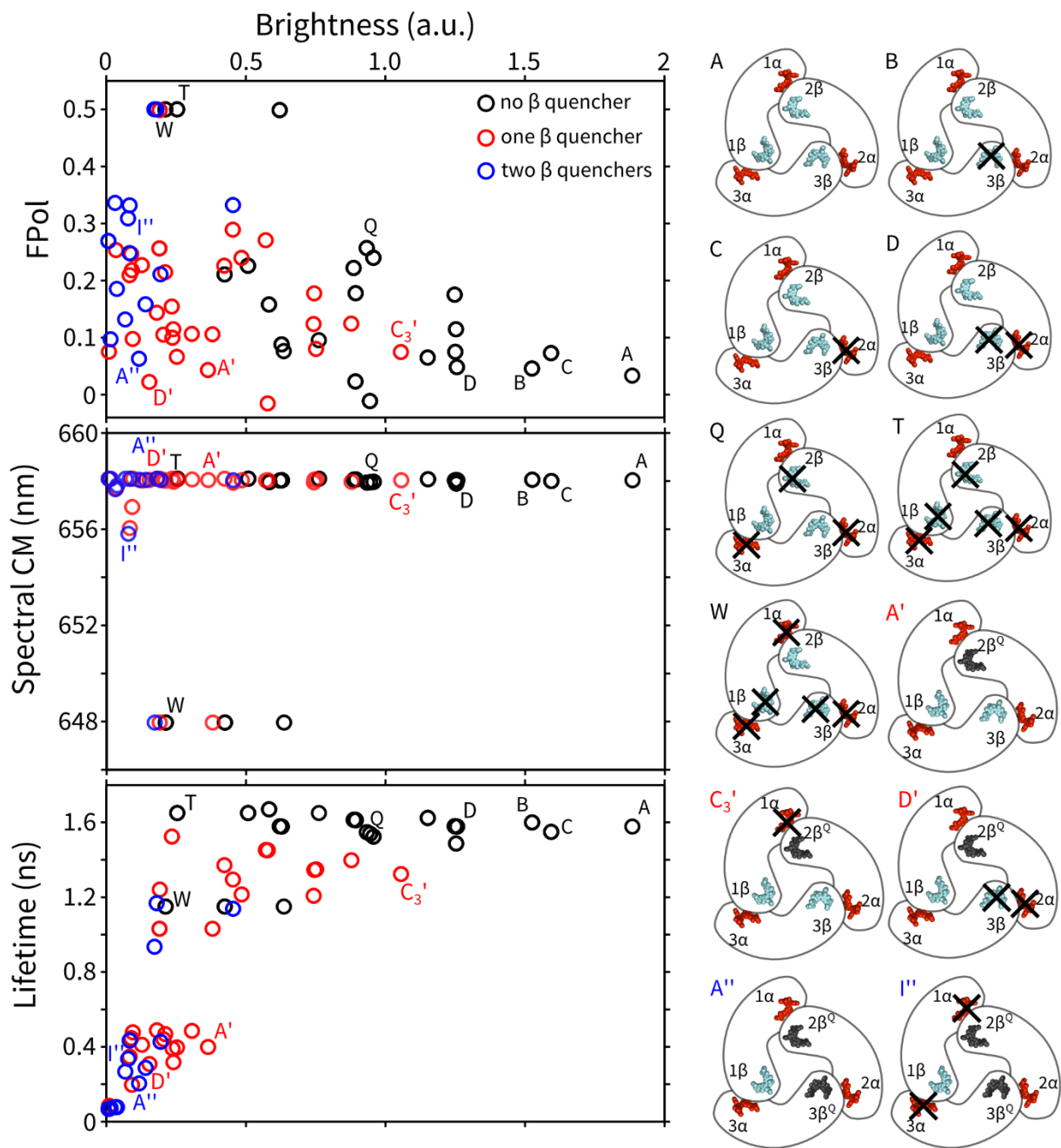


Fig. S9. Multi-parameter states of the trimer predicted by the emission model in the main text. States are color-grouped by the number of β quencher sites. The microscopic configuration of selected states are illustrated on the right. Black crosses indicate photobleached sites. Experimentally acquired brightness-FPoI and brightness-spectrum maps are illustrated in Fig. 4 of the main text. Experimentally acquired brightness-lifetime map can be found in Fig. 4 of ref. (8).

SI Tables

Table S1. FRET rates (ns^{-1}) in an intact trimer, based on site properties measured in this work and the crystal structure in ref. (34).

| acceptor donor | 1a | 1b | 2a | 2b | 3a | 3b |
|-------------------|------|------|------|------|------|------|
| 1a | - | 1.9 | 1.5 | 270 | 1.5 | 0.22 |
| 1b | 16 | - | 1.8 | 2.6 | 2300 | 2.6 |
| 2a | 1.5 | 0.22 | - | 1.9 | 1.5 | 270 |
| 2b | 2300 | 2.6 | 16 | - | 1.8 | 2.6 |
| 3a | 1.5 | 270 | 1.5 | 0.22 | - | 1.9 |
| 3b | 1.8 | 2.6 | 2300 | 2.6 | 16 | - |

References

1. Wang Q & Moerner WE (2014) Single-molecule motions enable direct visualization of biomolecular interactions in solution. *Nat Methods* 11: 555-558.
2. Trinquet E, Maurin F, Pr audat M & Mathis G (2001) Allophycocyanin 1 as a near-infrared fluorescent tracer: Isolation, characterization, chemical modification, and use in a homogeneous fluorescence resonance energy transfer system. *Anal Biochem* 296: 232-244.
3. Wang Q & Moerner WE (2012) Lifetime and spectrally resolved characterization of the photodynamics of single fluorophores in solution using the anti-Brownian electrokinetic trap. *J Phys Chem B* 117: 4641-4648.
4. Wang Q & Moerner WE (2010) Optimal strategy for trapping single fluorescent molecules in solution using the ABEL trap. *Appl Phys B* 99: 23-30.
5. Fields AP & Cohen AE (2012) Optimal tracking of a Brownian particle. *Opt Express* 20: 22589-22601.
6. Fore S, Laurence TA, Hollars CW & Huser T (2007) Counting constituents in molecular complexes by fluorescence photon antibunching. *IEEE J Select Topics Quantum Electron* 13: 996-1005.

7. Kurtsiefer C, Zarda P, Mayer S & Weinfurter H (2001) The breakdown flash of silicon avalanche photodiodes-back door for eavesdropper attacks?. *J Mod Opt* 48: 2039-2047.
8. Goldsmith RH & Moerner WE (2010) Watching conformational- and photodynamics of single fluorescent proteins in solution. *Nat Chem* 2(3): 179-186.
9. Wang Q (2015) Enabling multivariate investigation of single-molecule dynamics in solution by counteracting Brownian motion. *PhD Thesis, Stanford University*
10. Watkins LP & Yang H (2005) Detection of intensity change points in time-resolved single-molecule measurements. *J Phys Chem B* 109: 617-628.
11. Zander C, *et al.* (1996) Detection and characterization of single molecules in aqueous solution. *Appl Phys B* 63: 517-523.
12. Laurence TA, Fore S & Huser T (2006) Fast, flexible algorithm for calculating photon correlations. *Opt Lett* 31(6): 829-831.
13. Lidke K, Rieger B, Lidke D & Jovin T (2005) The role of photon statistics in fluorescence anisotropy imaging. *IEEE Trans Image Processing* 14: 1237-1245.
14. Axelrod D (1979) Carbocyanine dye orientation in red cell membrane studied by microscopic fluorescence polarization. *Biophys J* 26(3): 557-573.
15. Koshioka M, Sasaki K & Masuhara H (1995) Time-dependent fluorescence depolarization analysis in three-dimensional microspectroscopy. *Appl Spectrosc* 49: 224-228.
16. Fourkas JT (2001) Rapid determination of the three-dimensional orientation of single molecules. *Opt Lett* 26(4): 211-213.
17. Börner R, Kowerko D, Krause S, von Borczyskowski C & Hübner CG (2012) Efficient simultaneous fluorescence orientation, spectrum, and lifetime detection for single molecule dynamics. *J Chem Phys* 137: 164202.
18. Lakowicz JR (2006) *Principles of Fluorescence Spectroscopy*, (Springer, New York)
19. Parson WW (2007) *Modern Optical Spectroscopy: With Exercises and Examples from Biophysics and Biochemistry*, (Springer-Verlag Berlin Heidelberg)
20. Lounis BL, Deich J, Rosell FI, Boxer SG & Moerner WE (2001) Photophysics of DsRed, a red fluorescent protein, from the ensemble to the single-molecule level. *J Phys Chem B* 105: 5048-5054.
21. Barzda V, *et al.* (2001) Singlet-singlet annihilation kinetics in aggregates and trimers of LHCII. *Biophys J* 80: 2409-2421.
22. Gulbinas V, *et al.* (1996) Singlet-singlet annihilation and local heating in FMO complexes. *J Phys Chem* 100(45): 17950-17956.

23. De Schryver FC, *et al.* (2005) Energy dissipation in multichromophoric single dendrimers. *Acc Chem Res* 38: 514-522.
24. Tinnefeld P, *et al.* (2002) Antibunching in the emission of a single tetrachromophoric dendritic system. *J Am Chem Soc* 124: 14310-14311.
25. Han JJ, Kiss C, Bradbury ARM & Werner JH (2012) Time-resolved, confocal single-molecule tracking of individual organic dyes and fluorescent proteins in three dimensions. *ACS Nano* 6: 8922-8932.
26. Riter RR, Edington MD & Beck WF (1996) Protein-matrix solvation dynamics in the α subunit of C-phycoyanin. *J Phys Chem* 100: 14198-14205.
27. Shiu YJ, *et al.* (2002) A transient absorption study of allophycocyanin. *Proc Indian Acad Sci (Chem Sci)* 6: 611-621.
28. Sánchez-Mosteiro G, *et al.* (2004) Photon antibunching proves emission from a single subunit in the autofluorescent protein DsRed. *ChemPhysChem* 5: 1782-1785.
29. Kirilovsky D (2014) Modulating energy arriving at photochemical reaction centers: Orange carotenoid protein-related photoprotection and state transitions. *Photosynth Res* DOI: 10.1007/s11120-014-0031-7.
30. Tian L, *et al.* (2011) Site, rate, and mechanism of photoprotective quenching in cyanobacteria. *J Am Chem Soc* 133: 18304-18311.
31. Zhang H, *et al.* (2014) Molecular mechanism of photoactivation and structural location of the cyanobacterial orange carotenoid protein. *Biochemistry* 53: 13-19.
32. Stadnichuk IN, *et al.* (2015) Electronic coupling of the phycobilisome with the orange carotenoid protein and fluorescence quenching. *Photosynth Res* DOI: 10.1007/s11120-015-0148-3
33. Bailey S & Grossman A (2008) Photoprotection in cyanobacteria: Regulation of light harvesting. *Photochem Photobiol* 84: 1410-1420.
34. Brejc K, Ficner R, Huber R & Steinbacher S (1995) Isolation, crystallization, crystal structure analysis and refinement of allophycocyanin from the cyanobacterium *spirulina platensis* at 2.3 Å resolution. *J Mol Biol* 249(2): 424-440.